

Nucleon sigma terms with a variational analysis from Lattice QCD

Lorenzo Barca,^{1,*} Gunnar Bali,^{2,†} and Sara Collins^{2,‡}

¹*John von Neumann-Institut für Computing (NIC),*

Deutsches Elektronen-Synchrotron (DESY), Platanenallee 6, 15738 Zeuthen, Germany

²*Fakultät für Physik, Universität Regensburg, Universitätsstraße 31, 93053 Regensburg, Germany*

(Dated: 18th December 2024)

We determine the nucleon-sigma terms from lattice QCD. We find that the dominant excited state contamination in the nucleon three-point function with a scalar current is due to the transition between the nucleon and a S-wave scattering state of a nucleon and a scalar (sigma) meson. In this proof-of-concept study, we analyse a single $N_f = 3$ ensemble with the unphysically large pion mass $M_\pi = 429$ MeV. Excited state contamination is substantially reduced compared to the standard method when employing nucleon-sigma type interpolating operators within a generalised eigenvector analysis.

I. INTRODUCTION

Almost all visible matter of the universe is composed of nucleons, i.e. protons and neutrons. Most of the nucleons' mass can be attributed to the spontaneous breaking of chiral symmetry. Only a small part is due to the Higgs mechanism, i.e. the masses of the valence and sea quarks. These contributions can be quantified in a scheme- and gauge-invariant way in terms of scalar matrix elements, the quark-nucleon σ -terms,

$$\sigma_{qN} = m_q \langle N | \bar{q}q | N \rangle = m_q \frac{\partial m_N}{\partial m_q}, \quad (1)$$

where $q \in \{u, d, s, \dots\}$. These determine the coupling strength of the Standard Model Higgs boson (or other scalar particles) at zero recoil to the nucleon and are therefore important for theory predictions relevant for the direct detection of weakly interacting massive dark matter particles, see, e.g., the review [1].

In the isospin symmetric limit, i.e. for equal up and down quark masses $m_u = m_d$ and electric charges, the pion-nucleon σ -terms $\sigma_{\pi N} = \sigma_{uN} + \sigma_{dN}$ are the same for the proton and the neutron: $\sigma_{\pi p} = \sigma_{\pi n}$. $\sigma_{\pi N}$ can be extracted indirectly via dispersive analyses of pion-nucleon scattering data, employing low energy theorems and chiral perturbation theory (ChPT). Initially, a value $\sigma_{\pi N} = 45(8)$ MeV [2] was obtained. More recent phenomenological determinations, when corrected for isospin breaking effects [3], scatter around 56 MeV [3–7]. The σ -terms can also be determined from first principles lattice QCD, either directly [8–11] or indirectly [12–16] from the quark- (or the pseudoscalar meson mass-) dependence of the nucleon mass, using the second equality of Eq. (1). The most recent Flavour Lattice Averaging Group (FLAG) average of results obtained via the direct and the indirect methods, reads for the $N_f = 2 + 1$

theory $\sigma_{\pi N} = 42.2(2.4)$ MeV [17]. No tension is seen between the individual determinations. In contrast, the $N_f = 2 + 1 + 1$ average reads $\sigma_{\pi N} = 60.9(6.5)$ MeV [17]. This average, which is closer to the recent phenomenological estimates, is dominated by the PNDME result [10], obtained via the direct method.

Nucleon matrix elements, including the scalar matrix elements, are extracted from combinations of Euclidean two- and three-point functions. Within these, interpolating operators (interpolators) with the quantum numbers of the nucleon at a given three-momentum are used to create and to destroy hadronic states that propagate in Euclidean time. In the three-point function, a local quark bilinear current is inserted at an intermediate time. The interpolators not only create the ground state of interest but also excited states, including a tower of multi-particle states composed of a baryon and mesons. The ground state properties of interest can in principle be obtained in the limit of large Euclidean time separations between the “source”, the current (in the case of three-point functions) and the “sink”. Due to the exponential noise over signal problem of baryonic Green functions [18, 19], excited state contributions are often still significant for the separations that are achievable within reasonable precision. These are then accounted for by carrying out multi-exponential fits. Within three-point functions, the transitions between the ground and some excited states can be particularly enhanced since the current can directly create a meson which, in combination with a baryon, can give the quantum numbers of the final state nucleon. The transition from N states to $N\pi$ and $N\pi\pi$ states, mediated by a current, has been investigated using ChPT [10, 20–23]. Results of such calculations have then inspired the fit ansätze used in lattice analyses, e.g., of axial and pseudoscalar form factors [24, 25] and σ -terms [10, 11].

Motivated by ChPT, PNDME [10] constrain the gap between the ground and the first excited state energies to agree within 20% with the difference between the nucleon mass and the lowest possible non-interacting $N\pi$ (P-wave) or $N\pi\pi$ (S-wave) energy level. In their multi-state analysis this has a large impact, in particular, at

* lorenzo.barca@desy.de

† gunnar.bali@ur.de

‡ sara.collins@ur.de

small pion masses and for the disconnected quark line Wick contraction, resulting in the final value $\sigma_{\pi N} = 59.6(7.4)$ MeV. This is larger than what was found in other recent direct determinations [8–11] or predictions using the indirect (Feynman-Hellmann) method [13–15], with different systematics related to excited states.

A more systematic approach would be to explicitly resolve and subtract the dominant excited state contributions using a variational approach with a basis of interpolators, including baryon-meson type operators. The efficacy of this approach was first demonstrated in [26] at unphysically large pion masses, where the contributions from the lowest $N\pi$ excited states were removed from axial and pseudoscalar three-point functions with and without momentum transfer.¹ Subsequently, in [27] this was confirmed at the physical pion mass and extended to vector, tensor and scalar matrix elements. In the latter case no improvement was found when adding the lowest P-wave nucleon-pion type operator to the interpolator basis. This may not be surprising since one would expect flavour-diagonal scalar currents to dominantly couple to isoscalar scalar meson resonances. At the physical point this would be the $f_0(500)$ (decaying into $\pi\pi$) and the $f_0(980)$. In terms of the flavour content, these are mixtures of the scalar $I = I_3 = S = 0$ singlet and octet SU(3) eigenstates σ_0 and σ_8 , respectively.

Restricting ourselves to the baryon-(single)meson sector, a number of interpolators with the quantum numbers of a nucleon at rest can be constructed. These include P-wave combinations of type $N\pi$, $N\eta_0$, $N\eta_8$, ΣK etc. as well as S-wave combinations like Na_0 , $N\sigma_0$, $N\sigma_8$, ΣK_0^* and so on. To resolve the dominant multi-particle excited state it may be sufficient just to employ interpolators containing flavour-diagonal scalar mesons since only these can be created directly by the $\bar{u}u + \bar{d}d$ and $\bar{s}s$ currents of interest. These are the σ_0 and σ_8 mesons with flavour content $(\bar{u}u + \bar{d}d + \bar{s}s)/\sqrt{3}$ and $(\bar{u}u + \bar{d}d - 2\bar{s}s)/\sqrt{6}$, respectively. In addition we consider a $N\sigma$ interpolator with $\sigma \sim (\bar{u}u + \bar{d}d)/\sqrt{2}$.

In this proof-of-concept study, we investigate whether excited state contamination for scalar matrix elements can indeed be reduced in a variational approach, including either $N\sigma$ or $N\sigma_0$ and $N\sigma_8$ type interpolators in the basis. This work is carried out on a single Coordinated Lattice Simulations [28] ensemble employing $N_f = 3$ non-perturbatively improved Wilson fermions at a larger than physical pion mass² $M_\pi \approx 429$ MeV on the SU(3) flavour symmetric line ($m_q = m_u = m_d = m_s$, i.e., $M_K = M_\pi$) and a lattice spacing $a \approx 0.098$ fm. For this quark mass combination the σ_0 meson is stable with the mass $M_{\sigma_0} = 554(49)$ MeV (see the Supplemental Material), similar to the real part of the pole of the $f_0(500)$ observed in nature. We remark that the variational approach with

a basis of N and $N\sigma$ type interpolators (along with, e.g., $N\pi$ interpolators) has been investigated previously in the context of scattering studies [29, 30].

This Letter is organised as follows. In Sec. II we introduce the general procedure for the direct determination of the renormalized σ -terms. We then detail our variational determination of the energy eigenvalues and eigenvectors in Sec. III and compare results from fits to the improved and standard Green functions in Sec. IV, before we conclude in Sec. V.

II. DIRECT DETERMINATION OF THE σ -TERMS

The scalar matrix elements can be extracted from two- and three-point functions

$$C_{2\text{pt}}(t) = \langle O(t)\bar{O}(0) \rangle, \quad (2)$$

$$C_{3\text{pt}}^{\mathcal{S}^q}(t, \tau) = \langle O(t)\mathcal{S}^q(\tau)\bar{O}(0) \rangle, \quad (3)$$

in the rest frame. The interpolating operator \bar{O} (O) creates (annihilates) states with the quantum numbers of the nucleon $I(J^P) = \frac{1}{2}(\frac{1}{2}^+)$ at the source on timeslice 0 (sink on timeslice t). For the three-point function, the scalar current $\mathcal{S}^q = \bar{q}q$ is inserted at an intermediate time τ , where we consider the flavour combinations $\mathcal{S}^{u+d} = \bar{u}u + \bar{d}d$ and $\mathcal{S}^s = \bar{s}s$. The spectral decomposition of the correlation functions reads

$$C_{2\text{pt}}(t) = \sum_n |Z_n|^2 e^{-E_n t}, \quad (4)$$

$$C_{3\text{pt}}^{\mathcal{S}^q}(t, \tau) = \sum_{n', n} Z_{n'} \bar{Z}_n \langle n' | \mathcal{S}^q | n \rangle e^{-E_{n'}(t-\tau)} e^{-E_n \tau}. \quad (5)$$

E_n is the energy of state $|n\rangle$, created by the interpolator \bar{O} from the vacuum state $|\Omega\rangle$, and \bar{Z}_n is the associated overlap factor $\bar{Z}_n \propto \langle n | \bar{O} | \Omega \rangle$. In the limit of large time separations $t \gg \tau \gg 0$, the ground state contribution ($n = n' = N$) dominates. By performing fits to combinations of the two- and three-point functions (see Sec. IV) the nucleon scalar matrix elements in the lattice scheme can be extracted:

$$\langle N | \mathcal{S}^{u+d} | N \rangle = \bar{u}_N g_S^{\text{lat}, u+d} u_N, \quad (6)$$

$$\langle N | \mathcal{S}^s | N \rangle = \bar{u}_N g_S^{\text{lat}, s} u_N. \quad (7)$$

The Lorentz decomposition of these matrix elements is expressed in terms of the scalar charges $g_S^{\text{lat}, q}$, $q \in \{u, d, s\}$, and u_N , the spinor of a nucleon at rest. For Wilson fermions, on the SU(3) flavour symmetric line the renormalised σ -terms are given by

$$\sigma_{\pi N} = m_q \left[r_m g_S^{\text{lat}, u+d} + \frac{2}{3}(1 - r_m) g_S^{\text{lat}, u+d+s} \right], \quad (8)$$

$$\sigma_{sN} = m_q \left[r_m g_S^{\text{lat}, s} + \frac{1}{3}(1 - r_m) g_S^{\text{lat}, u+d+s} \right], \quad (9)$$

¹ No improvement was seen in the forward limit, in the rest frame.

² The trace of the mass matrix $m_u + m_d + m_s$ is close to that at the physical point.

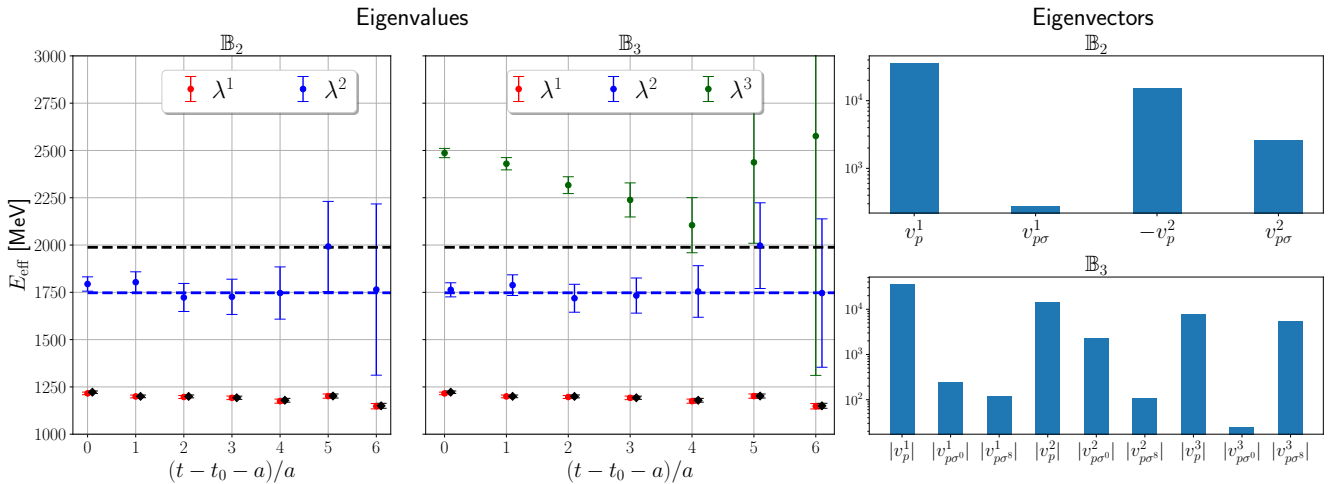


Figure 1: Effective energies obtained from the GEVP with interpolator bases \mathbb{B}_2 (left) and \mathbb{B}_3 (middle) for $t_0 = 3a$, compared to the effective mass of the standard nucleon two-point function (black diamonds) constructed from the O_p operators. The dashed lines correspond to the energies of the non-interacting S-wave $N\sigma$ (blue) and lowest P-wave $N\pi$ (black) levels. Also shown are the corresponding generalised eigenvector components for $t - t_0 = 3a$ for \mathbb{B}_2 (right top) and \mathbb{B}_3 (right bottom).

where m_q is the vector Ward identity quark mass and r_m is the ratio of the singlet to non-singlet mass renormalisation factors. In our case, $r_m = 3.409(57)$ [31] and $m_q = 6.62(25)$ MeV [15].

III. VARIATIONAL ANALYSIS

To construct an interpolator with large overlap to the nucleon ground state, we perform a variational analysis [32]. We utilise two bases of interpolators with proton quantum numbers ($I_z = +1/2$). Basis $\mathbb{B}_2 = \{O_p, O_{p\sigma}\}$ comprises the usual proton interpolator $O_p = u^T(dC\gamma_5 u)$ and a S-wave proton-sigma meson interpolator $O_{p\sigma}$, combining O_p with the SU(2) sigma meson operator ($I = 0$, $J^{PC} = 0^{++}$), $O_\sigma = (\bar{u}u + \bar{d}d)/\sqrt{2}$. For basis $\mathbb{B}_3 = \{O_p, O_{p\sigma_0}, O_{p\sigma_8}\}$, we implement the SU(3) singlet and octet sigma meson operators, $O_{\sigma_0} = (\bar{u}u + \bar{d}d + \bar{s}s)/\sqrt{3}$ and $O_{\sigma_8} = (\bar{u}u + \bar{d}d - 2\bar{s}s)/\sqrt{6}$, respectively. To improve the overlap with lower-lying levels, we construct spatially extended interpolators by Wuppertal smearing [33, 34] the quark fields, incorporating APE smeared links [35]. For the nucleon and σ interpolators we employ the smearing radii $\langle r^2 \rangle^{1/2} \sim 1.0$ fm and $\langle r^2 \rangle^{1/2} \sim 0.2$ fm, respectively.

Using these bases, we build the following matrices of two-point functions:

$$\mathbb{C}_{2\text{pt}}(t)_{ij} = \langle O_i(t)\bar{O}_j(0) \rangle \quad (10)$$

with $O_i, O_j \in \mathbb{B}_2$ or \mathbb{B}_3 . The corresponding Wick contractions are evaluated using the sequential source method [36] for quark-line connected topologies. For the disconnected diagrams also stochastic estimation is

used, including the one-end-trick [37, 38], see the Supplemental Material. We solve the generalised eigenvalue problem (GEVP)

$$\mathbb{C}_{2\text{pt}}(t)\Lambda(t, t_0) = \mathbb{C}_{2\text{pt}}(t_0)V(t, t_0)\Lambda(t, t_0) \quad (11)$$

for different reference times t_0 and $t > t_0$. This gives the matrix of generalised eigenvalues $\Lambda(t, t_0) = \text{diag}(\lambda^\alpha(t, t_0))$ and eigenvectors $V(t, t_0) = (v_i^\alpha(t, t_0))$, where the superscripts (subscripts) refer to the eigenstate (operator) and we employ the normalisation $v^{\alpha\tau}\mathbb{C}_{2\text{pt}}(t_0)v^\beta = \delta^{\alpha\beta}$. In the limit of large times, the eigenvalues decay exponentially with the energy of the state, $\lambda^\alpha(t, t_0) \propto e^{-E_\alpha(t-t_0)}$, while the elements of the eigenvectors $v_i^\alpha(t, t_0)$ are related to the overlap of the operator O_i with the state α .

The effective energies $E_{\text{eff}}^\alpha(t) = a^{-1} \ln[\lambda^\alpha(t)/\lambda^\alpha(t+a)]$ are shown in Fig. 1 for $t_0 = 0.3$ fm. For both bases, the lowest energy coincides with the nucleon mass on this ensemble [15], while the second level is close to the sum of the nucleon and sigma energies. Therefore, we will identify $\alpha = 1$ with N and $\alpha = 2$ with $N\sigma$. The third eigenvalue for basis \mathbb{B}_3 does not exhibit a clear plateau, with the statistical errors increasing rapidly for $t-t_0-a > 3a$. We were not able to obtain a reliable estimate of the σ_8 meson mass, however, assuming the masses of the σ_8 and the physical $f_0(980)$ are similar (as is the case for σ_0 and $f_0(500)$), the $N\sigma_8$ non-interacting level would lie around 2200 MeV, above the almost degenerate lowest P-wave $N\pi$ and S-wave $N\pi\pi$ levels.

We observe that $E_{\text{eff}}^1(t)$ is consistent with the effective mass of the standard nucleon two-point function, $\mathbb{C}_{2\text{pt}}^{\text{STD}}(t) = \mathbb{C}_{2\text{pt}}(t)_{11} = \langle O_p(t)\bar{O}_p(0) \rangle$, see Fig. 1, which plateaus already at $t = 0.5$ fm (equal to $t - t_0 - a = a$ for $t_0 = 3a$).

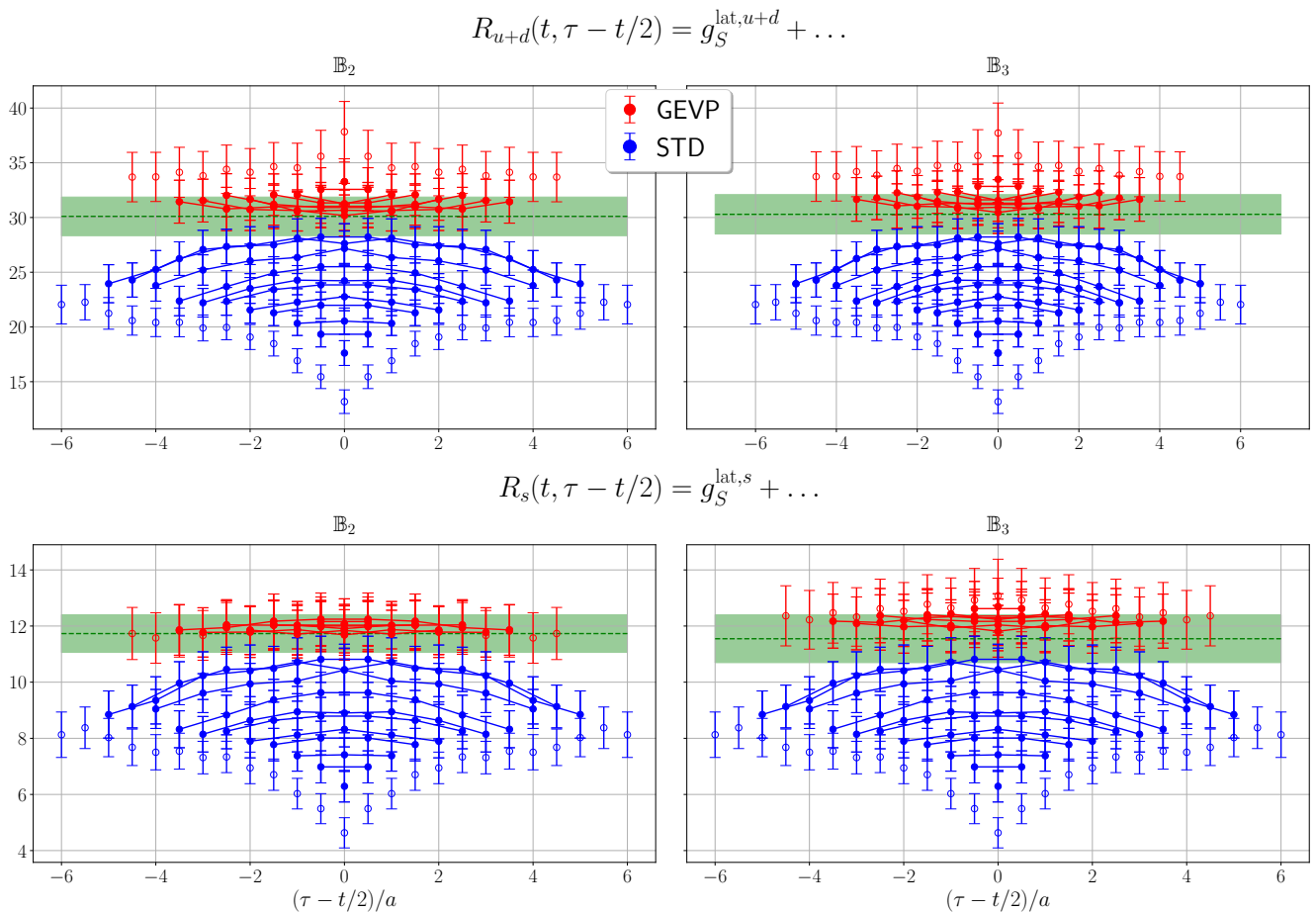


Figure 2: Results for the GEVP-improved ratios R_{u+d} (top) and R_s (bottom) for \mathbb{B}_2 (left) and \mathbb{B}_3 (right). The green dashed lines and bands show the central values and errors, respectively, of $g_S^{\text{lat}, u+d}$ (top) and $g_S^{\text{lat}, s}$ (bottom) extracted using the summation method, see Sec. IV. The standard ratios obtained using the interpolator O_p are shown for comparison. The data points that are utilised in the fits (Sec. IV) are indicated by solid circles.

The multi-particle interpolators contribute two orders of magnitude less to v^1 than O_p , however, the impact on three-point functions can still be significant, see below. Note that the O_p contribution also dominates v^2 (and v^3).

An operator with an improved overlap to the ground state can be constructed from a linear combination of the initial operators O_i and the eigenvectors for the first level $v_i^{\alpha=1}(t', t_0)$ evaluated at a large enough time t' such that the eigenvector is stable ($t \geq t' = 6a$ for $t_0 = 3a$ in our setup),

$$O^{\text{imp}}(t) \propto \sum_{i \in \mathbb{B}} v_i^{\alpha=1}(t', t_0) O_i(t - t_0/2), \quad (12)$$

with $\mathbb{B} = \mathbb{B}_2$ or \mathbb{B}_3 . This operator can be used to define GEVP-improved two- and three-point functions

$$C_{2\text{pt}}^{\text{imp}}(t) = \langle O^{\text{imp}}(t) \bar{O}^{\text{imp}}(0) \rangle, \quad (13)$$

$$C_{3\text{pt}}^{\text{imp}, S^q}(t, \tau) = \langle O^{\text{imp}}(t) S^q(\tau) \bar{O}^{\text{imp}}(0) \rangle. \quad (14)$$

We neglect the $N\sigma \xrightarrow{S^q} N\sigma$ contributions to $C_{3\text{pt}}^{\text{imp}, S^q}$ that

are suppressed by the second power of the small eigenvector component $v_{p\sigma}^1$ for \mathbb{B}_2 ($v_{p\sigma_0, p\sigma_s}^1$ for \mathbb{B}_3). In particular, we do not expect the matrix element $\langle N\sigma | S^q | N\sigma \rangle$ to be enhanced relative to $\langle N | S^q | N \rangle$. In order to assess the size of excited state contamination to the improved three-point function we form the ratio

$$R_{u+d, s}^{\text{GEVP}}(t, \tau) = \frac{C_{3\text{pt}}^{\text{imp}, S^{u+d, s}}(t, \tau)}{C_{2\text{pt}}^{\text{imp}}(t)} \quad (15)$$

for the S^{u+d} and S^s currents for 10 source-sink separations, $t = 2a - 11a = 0.2 - 1.1$ fm, shown in Fig. 2. Considering the spectral decomposition given in Sec. II, this ratio tends to the charges $g_S^{\text{lat}, u+d}$ and $g_S^{\text{lat}, s}$ of the nucleon, respectively, at large time separations. For comparison we also evaluate $R_{u+d, s}^{\text{STD}}(t, \tau)$, the ratio of the standard three-point function $C_{3\text{pt}}^{\text{STD}}(t, \tau) = \langle O_p(t) S^{u+d, s}(\tau) \bar{O}_p(0) \rangle$ to $C_{2\text{pt}}^{\text{STD}}(t)$ for $t = 2a - 17a = 0.2 - 1.7$ fm. Note that only the ratios up to $t = 14a$ are shown in the figure. The standard ratios show a significant dependence on the source-sink and current

Table I: Results for the unrenormalized nucleon scalar charges from the standard ratio $R_{u+d,s}^{\text{STD}}(t, \tau)$. These and the summed ratios (16) are fitted according to Eq. (19) and Eqs. (17) – (18), respectively. For the latter, the fit range is varied for each model and a weighted average is quoted, along with the range of the χ^2/dof . Where applicable, the energy gaps ΔE between the first excited state and the ground state are given. Priors for ΔE based on the non-interacting S-wave $N\sigma$ or P-wave $N\pi$ energies are labelled as $\Delta E_{N\sigma}$ and $\Delta E_{N\pi}$, respectively, see the text.

Fit models	$g_S^{\text{lat},u+d}$	ΔE [MeV]	χ^2/dof	$g_S^{\text{lat},s}$	ΔE [MeV]	χ^2/dof
Eq. (17) $c_{11} = 0$	31.7 ± 2.6	495 ± 191	[1.1, 1.3]	11.8 ± 1.0	526 ± 193	[1.1, 1.3]
Eq. (17) $c_{11} = 0, \Delta E_{N\sigma}$	30.8 ± 1.8	516 ± 35	[1.1, 1.4]	11.7 ± 0.9	514 ± 33	[1.1, 1.3]
Eq. (17) $c_{11} = 0, \Delta E_{N\pi}$	29.0 ± 1.6	678 ± 31	[1.2, 1.5]	10.9 ± 0.8	678 ± 30	[1.2, 1.4]
Eq. (18)	30.0 ± 2.0	–	[1.0, 1.4]	11.6 ± 0.9	–	[0.9, 1.5]
Eq. (19)	31.8 ± 2.6	566 ± 132	0.63	12.3 ± 0.9	537 ± 114	0.61
Eq. (19) $\Delta E_{N\sigma}$	31.6 ± 2.0	553 ± 52	0.63	12.2 ± 0.7	527 ± 40	0.61
Eq. (19) $\Delta E_{N\pi}$	29.5 ± 1.6	690 ± 39	0.65	11.2 ± 0.8	686 ± 32	0.64

insertion time, indicating large excited state contributions to the three-point function. In contrast, the GEVP ratios display a much milder dependence. This suggests that the S-wave $N\sigma$ contributions to $C_{3\text{pt}}^{\text{STD}}(t, \tau)$ are significant and that these are effectively removed when employing the GEVP-improved interpolator. However, clearly, residual excited state contamination remains and a larger basis of operators would need to be considered to reduce these contributions further.

IV. FITTING ANALYSIS

In the following, we present the fitting analysis carried out to extract the scalar charges from the ratios of the three-point to two-point correlation functions. With a large number of source-sink separations (t) at our disposal, we employ the summation method and compute

$$R_{u+d,s}^{\text{sum}}(t) = \sum_{\tau=c}^{t-c} R_{u+d,s}(t, \tau), \quad (16)$$

where the sum over the current insertion (τ) runs from timeslice $\tau = c$ up to $t - c$. Considering the spectral decompositions in Eqs. (4) and (5) truncated after the first excited state, the t -dependence of the summed ratio reads

$$R_{u+d,s}^{\text{sum}}(t) = g_S^{\text{lat},u+d,s}(t - 2c + a) + 2c_{10} \frac{e^{\Delta E(c-t)} - e^{\Delta E(a-c)}}{1 - e^{\Delta E}} + c_{11}(t - 2c + a)e^{-\Delta Et}. \quad (17)$$

The coefficients c_{10} and c_{11} are related to the matrix elements $\langle N | \mathcal{S}^{u+d,s} | 2 \rangle$ and $\langle 2 | \mathcal{S}^{u+d,s} | 2 \rangle$, respectively, and ΔE denotes the energy gap between the ground $|N\rangle = |1\rangle$ and the first resolvable excited state $|2\rangle$. In the limit of ground state dominance, this dependence simplifies to

$$R_{u+d,s}^{\text{sum}}(t) = c_0 + g_S^{\text{lat},u+d,s} t \quad (18)$$

with $c_0 = g_S^{u+d,s}(a - 2c)$.

First, we discuss the fits to the standard ratios $R_{u+d,s}^{\text{STD}}(t, \tau)$. Given the significant excited state contributions for smaller t seen in Fig. 2, we perform correlated fits to the summed ratios employing Eq. (17) with $c = 2a$. The latter means that the summed ratio is realised for $t \geq 4a$. We set $c_{11} = 0$ as the term involving the excited-state to excited state transition was not resolved. The fit range is varied and we take a weighted average of the results.³ The values obtained for $g_S^{u+d,s}$ and ΔE are listed in Tab. I. The energy gap is not well determined in the fits, however, we know from the GEVP analysis (see Fig. 1) that the first excited state energy is consistent with the S-wave $N\sigma$ non-interacting level. This motivates us to repeat the analysis imposing a prior on ΔE equal to the mass of the sigma meson with a width of 50 MeV (9%), leading to similar results for the scalar charges but with smaller uncertainties. In the absence of detailed knowledge of the energy spectrum, a prior for the energy gap is often set using the P-wave $N\pi$ energy (although additional excited states are usually taken into account in the fit model). A larger energy gap gives consistent but slightly lower values for the scalar charges. For $t \geq 8a$ we are also able to perform linear fits (18) (see Tab. I) since the excited state contributions to $R_{u+d,s}^{\text{sum}}$ fall below the noise.

For completeness, we also carried out correlated fits to $R_{u+d,s}^{\text{STD}}(t, \tau)$ with the following ansatz:

$$R_{u+d,s}(t, \tau) = g_S^{\text{lat},u+d,s} + c_{10} \left(e^{-\Delta E(t-\tau)} + e^{-\Delta E\tau} \right), \quad (19)$$

where, again, the excited-state to excited-state term is omitted. We simultaneously fit the ratios with $t/a =$

³ The weighted average \bar{a} of fit coefficient $a \in \{g_S^{u+d,s}, \Delta E\}$ is computed using weights $w_i = N \exp(-(\chi_i^2 - \text{dof}_i)/2)$, where χ_i^2 and dof_i are the fit quality and number of degrees of freedom for fit i , respectively. N is chosen so that $\sum_i w_i = 1$. The average \bar{a} and its uncertainty Δa are given by $\bar{a} = \sum_i w_i a_i$ and $\Delta a^2 = \sum_i w_i \Delta a_i^2$, where Δa_i is the bootstrapped error for fit i .

8, 9, 11, 13, 15 employing the fit range $2a \leq \tau \leq t - 2a$ for each t .⁴ The largest source-sink separations are not included in the fit due to the deterioration in the signal (note that the summed ratios display smooth behaviour up to $t = 17a$). The results, detailed in Tab. I, are compatible with those for the summed ratios.

Turning to the GEVP-improved summed ratios (again with $c = 2a$, $t \geq 4a$), we find that the excited state contributions are sufficiently suppressed to employ the linear fit ansatz (18) starting from $t = 4a$. The final results for the weighted averages for basis \mathbb{B}_2 are

$$\begin{aligned} g_S^{\text{lat},u+d} &= 30.1 \pm 1.8 & [1.0, 0.8, 1.0] \\ g_S^{\text{lat},s} &= 11.7 \pm 0.7 & [1.0, 1.2, 1.3]. \end{aligned} \quad (20)$$

The χ^2/dof for the three fits which enter the average (with fit ranges $t/a = 4 - 11$, $t/a = 5 - 11$ and $t/a = 6 - 11$) are given in brackets. For \mathbb{B}_3 , we obtain

$$\begin{aligned} g_S^{\text{lat},u+d} &= 30.3 \pm 1.8 & [1.1, 0.8, 1.1] \\ g_S^{\text{lat},s} &= 11.6 \pm 0.9 & [1.1, 0.9, 1.2] \end{aligned} \quad (21)$$

for the same fit ranges. These four fit results for the charges are displayed as the green bands in Fig. 2. The standard and GEVP summed ratios are shown in Fig. S3 of the Supplemental Material, along with representative fits utilising Eqs. (17) and (18).

V. SUMMARY AND DISCUSSION

We utilised the variational approach with a basis including nucleon-sigma type interpolators to remove the dominant excited state contamination from the three-point correlation functions with a scalar current. The scalar charges are reliably extracted from source-sink separations $t \leq 1.1$ fm. The results of the standard method (Tab. I) agree well with the GEVP-improved

numbers (20) and (21), however, the former require larger time separations (see also the comparison in Fig. 2). Considering the exponential increase in the noise over signal with t , we find the new method to be cost effective. Converting our values via Eqs. (8) and (9) into the σ -terms, we obtain $\sigma_{\pi N} = (235 \pm 24)$ MeV and $\sigma_{sN} = (42 \pm 16)$ MeV, where the large uncertainty, in particular for σ_{sN} , is mostly due to the large value of r_m at our coarse lattice spacing $a \approx 0.098$ fm ($r_m \approx 3.4$ [31]). The results are consistent with those at similar pion masses from other works [8, 39].

For physical quark masses, the σ meson becomes unstable and one might be tempted to perform a full scattering analysis [40–46], including $N\pi\pi$ type interpolators. However, since the width of the $f_0(500)$ is similar to its energy [47], also a scalar bilinear interpolator will most likely couple well to the scattering states [29, 30, 48], as well as to the local isoscalar current. Therefore, the method presented here may very well be directly applicable to the physical point. Future studies with closer to physical pion masses will shed further light on this.

ACKNOWLEDGMENTS

We thank P. Petrak for sharing results on the sigma terms with us. L. B. is grateful to his colleagues at DESY and at the Humboldt University for stimulating discussions, with special thanks to J. Green and R. Sommer for their insightful comments. He also extends his gratitude to R. Gupta and K.-F. Liu and the members of the χ QCD collaboration for useful discussions. G. B. thanks S. Leupold for discussions. L. B. received support through the German Research Foundation (DFG) research unit FOR5269 “Future methods for studying confined gluons in QCD”. Simulations were performed on the QPACE 3 computer of SFB/TRR-55, using an adapted version of the CHROMA [49] software package.

-
- [1] J. M. Alarcón, Brief history of the pion–nucleon sigma term, *Eur. Phys. J. ST* **230**, 1609 (2021), arXiv:2205.01108 [hep-ph].
- [2] J. Gasser, H. Leutwyler, and M. E. Sainio, Sigma term update, *Phys. Lett. B* **253**, 252 (1991).
- [3] M. Hoferichter, J. Ruiz de Elvira, B. Kubis, and U.-G. Meißner, On the role of isospin violation in the pion–nucleon σ -term, *Phys. Lett. B* **843**, 138001 (2023), arXiv:2305.07045 [hep-ph].
- [4] J. M. Alarcón, J. M. Camalich, and J. A. Oller, The chiral representation of the πN scattering amplitude and the pion–nucleon sigma term, *Phys. Rev. D* **85**, 051503 (2012), arXiv:1110.3797 [hep-ph].

- [5] Y.-H. Chen, D.-L. Yao, and H. Q. Zheng, Analyses of pion–nucleon elastic scattering amplitudes up to $O(p^4)$ in extended-on-mass-shell subtraction scheme, *Phys. Rev. D* **87**, 054019 (2013), arXiv:1212.1893 [hep-ph].
- [6] M. Hoferichter, J. Ruiz de Elvira, B. Kubis, and U.-G. Meißner, High-precision determination of the pion–nucleon σ term from Roy-Steiner equations, *Phys. Rev. Lett.* **115**, 092301 (2015), arXiv:1506.04142 [hep-ph].
- [7] J. Ruiz de Elvira, M. Hoferichter, B. Kubis, and U.-G. Meißner, Extracting the σ -term from low-energy pion–nucleon scattering, *J. Phys. G* **45**, 024001 (2018), arXiv:1706.01465 [hep-ph].
- [8] Y.-B. Yang, A. Alexandru, T. Draper, J. Liang, and K.-F. Liu (χ QCD Collaboration), πN and strangeness sigma terms at the physical point with chiral fermions, *Phys. Rev. D* **94**, 054503 (2016), arXiv:1511.09089 [hep-lat].
- [9] G. S. Bali, S. Collins, D. Richtmann, A. Schäfer, W. Söld-

⁴ For our setup, with 800 configurations employed in the analysis, this choice ensures that the covariance matrix is well determined.

- ner, and A. Sternbeck (RQCD Collaboration), Direct determinations of the nucleon and pion σ terms at nearly physical quark masses, *Phys. Rev. D* **93**, 094504 (2016), arXiv:1603.00827 [hep-lat].
- [10] R. Gupta, S. Park, M. Hoferichter, E. Mereghetti, B. Yoon, and T. Bhattacharya, Pion–nucleon sigma term from Lattice QCD, *Phys. Rev. Lett.* **127**, 242002 (2021), arXiv:2105.12095 [hep-lat].
- [11] A. Agadjanov, D. Djukanovic, G. von Hippel, H. B. Meyer, K. Ottnad, and H. Wittig, Nucleon sigma terms with $N_f = 2 + 1$ flavors of $O(a)$ -improved Wilson fermions, *Phys. Rev. Lett.* **131**, 261902 (2023), arXiv:2303.08741 [hep-lat].
- [12] C. Alexandrou, V. Drach, K. Jansen, C. Kallidonis, and G. Koutsou, Baryon spectrum with $N_f = 2 + 1 + 1$ twisted mass fermions, *Phys. Rev. D* **90**, 074501 (2014), arXiv:1406.4310 [hep-lat].
- [13] S. Dürr *et al.* (Budapest-Marseille-Wuppertal Collaboration), Lattice computation of the nucleon scalar quark contents at the physical point, *Phys. Rev. Lett.* **116**, 172001 (2016), arXiv:1510.08013 [hep-lat].
- [14] S. Borsanyi, Z. Fodor, C. Hoelbling, L. Lellouch, K. K. Szabo, C. Torrero, and L. Varnhorst, Ab-initio calculation of the proton and the neutron’s scalar couplings for new physics searches, arXiv:2007.03319 [hep-lat] (2020).
- [15] G. S. Bali, S. Collins, P. Georg, D. Jenkins, P. Korcyl, A. Schäfer, E. E. Scholz, J. Simeth, W. Söldner, and S. Weishäupl (RQCD Collaboration), Scale setting and the light baryon spectrum in $N_f = 2 + 1$ QCD with Wilson fermions, *J. High Energy Phys.* **2023** (05), 035, arXiv:2211.03744 [hep-lat].
- [16] B. Hu, X. Jiang, K.-F. Liu, P. Sun, and Y.-B. Yang (CLQCD Collaboration), Trace anomaly contributions to baryon masses from Lattice QCD, arXiv:2411.18402 [hep-lat] (2024).
- [17] Y. Aoki *et al.* (Flavour Lattice Averaging Group (FLAG)), FLAG Review 2024, arXiv:2411.04268 [hep-lat] (2024).
- [18] H. W. Hamber, E. Marinari, G. Parisi, and C. Rebbi, Considerations on numerical analysis of QCD, *Nucl. Phys. B* **225**, 475 (1983).
- [19] G. P. Lepage, The analysis of algorithms for lattice field theory, *in* From actions to answers. Proceedings, Theoretical Advanced Study Institute in Elementary Particle Physics, Boulder, CO, USA, June 5–30, 1989, eds. T. A. DeGrand and D. Toussaint, *World Scientific, Singapore*, 97 (1990).
- [20] B. C. Tiburzi, Time dependence of nucleon correlation functions in chiral perturbation theory, *Phys. Rev. D* **80**, 014002 (2009), arXiv:0901.0657 [hep-lat].
- [21] O. Bär, Nucleon-pion-state contribution in lattice calculations of the nucleon charges g_A , g_T and g_S , *Phys. Rev. D* **94**, 054505 (2016), arXiv:1606.09385 [hep-lat].
- [22] O. Bär, $N\pi$ -state contamination in lattice calculations of the nucleon axial form factors, *Phys. Rev. D* **99**, 054506 (2019), arXiv:1812.09191 [hep-lat].
- [23] O. Bär and H. Colic, $N\pi$ -state contamination in lattice calculations of the nucleon electromagnetic form factors, *Phys. Rev. D* **103**, 114514 (2021), arXiv:2104.00329 [hep-lat].
- [24] G. S. Bali, L. Barca, S. Collins, M. Gruber, M. Löffler, A. Schäfer, W. Söldner, P. Wein, S. Weishäupl, and T. Wurm (RQCD Collaboration), Nucleon axial structure from lattice QCD, *J. High Energy Phys.* **2020** (05), 126, arXiv:1911.13150 [hep-lat].
- [25] Y.-C. Jang, R. Gupta, T. Bhattacharya, B. Yoon, and H.-W. Lin (PNDME Collaboration), Nucleon isovector axial form factors, *Phys. Rev. D* **109**, 014503 (2024), arXiv:2305.11330 [hep-lat].
- [26] L. Barca, G. Bali, and S. Collins, Toward N to $N\pi$ matrix elements from lattice QCD, *Phys. Rev. D* **107**, L051505 (2023), arXiv:2211.12278 [hep-lat].
- [27] C. Alexandrou, G. Koutsou, Y. Li, M. Petschlies, and F. Pittler, Investigation of pion-nucleon contributions to nucleon matrix elements, arXiv:2408.03893 [hep-lat] (2024).
- [28] M. Bruno *et al.* (CLS), Simulation of QCD with $N_f = 2 + 1$ flavors of non-perturbatively improved Wilson fermions, *J. High Energy Phys.* **2015** (02), 043, arXiv:1411.3982 [hep-lat].
- [29] C. B. Lang, L. Leskovec, M. Padmanath, and S. Prelovsek, Pion-nucleon scattering in the Roper channel from Lattice QCD, *Phys. Rev. D* **95**, 014510 (2017), arXiv:1610.01422 [hep-lat].
- [30] A. L. Kiratidis, W. Kamleh, D. B. Leinweber, Z.-W. Liu, F. M. Stokes, and A. W. Thomas, Search for low-lying lattice QCD eigenstates in the Roper regime, *Phys. Rev. D* **95**, 074507 (2017), arXiv:1608.03051 [hep-lat].
- [31] J. Heitger, F. Joswig, P. L. J. Petrak, and A. Vladikas, Ratio of flavour non-singlet and singlet scalar density renormalisation parameters in $N_f = 3$ QCD with Wilson quarks, *Eur. Phys. J. C* **81**, 606 (2021), [Erratum: *Eur. Phys. J. C* **82**, 104 (2022)], arXiv:2101.10969 [hep-lat].
- [32] J. Bulava, M. Donnellan, and R. Sommer, On the computation of hadron-to-hadron transition matrix elements in lattice QCD, *J. High Energy Phys.* **2012** (01), 140, arXiv:1108.3774 [hep-lat].
- [33] S. Güsken, U. Löw, K. H. Mütter, R. Sommer, A. Patel, and K. Schilling, Nonsinglet axial vector couplings of the baryon octet in Lattice QCD, *Phys. Lett. B* **227**, 266 (1989).
- [34] S. Güsken, A study of smearing techniques for hadron correlation functions, *Nucl. Phys. B Proc. Suppl.* **17**, 361 (1990).
- [35] M. Falcioni, M. L. Paciello, G. Parisi, and B. Taglienti, Again on SU(3) glueball mass, *Nucl. Phys. B* **251**, 624 (1985).
- [36] L. Maiani, G. Martinelli, M. L. Paciello, and B. Taglienti, Scalar densities and baryon mass differences in lattice QCD with Wilson fermions, *Nucl. Phys. B* **293**, 420 (1987).
- [37] R. Sommer, Leptonic decays of B and D mesons, *Proceedings, 12th International Symposium on Lattice Field Theory (Lattice 94), Bielefeld, Germany, September 27–October 1, 1994*, *Nucl. Phys. Proc. Suppl.* **42**, 186 (1995), arXiv:hep-lat/9411024 [hep-lat].
- [38] M. Foster and C. Michael (UKQCD Collaboration), Hadrons with a heavy color adjoint particle, *Phys. Rev. D* **59**, 094509 (1999), arXiv:hep-lat/9811010 [hep-lat].
- [39] P. L. J. Petrak, G. Bali, S. Collins, J. Heitger, D. Jenkins, and S. Weishäupl, Sigma terms of the baryon octet in $N_f = 2 + 1$ QCD with Wilson quarks, *PoS LATTICE2022*, 112 (2023), arXiv:2301.03871 [hep-lat].
- [40] A. Briceño, R. J. Dudek, J. R. G. Edwards, and D. J. Wilson (Hadron Spectrum Collaboration), Isoscalar $\pi\pi$ scattering and the σ meson resonance from QCD, *Phys. Rev. Lett.* **118**, 022002 (2017), arXiv:1607.05900 [hep-ph].

- [41] L. Liu *et al.* (ETM Collaboration), Isospin-0 $\pi\pi$ s -wave scattering length from twisted mass lattice QCD, Phys. Rev. D **96**, 054516 (2017), arXiv:1612.02061 [hep-lat].
- [42] Z. Fu and X. Chen, $I = 0$ $\pi\pi$ s -wave scattering length from lattice QCD, Phys. Rev. D **98**, 014514 (2018), arXiv:1712.02219 [hep-lat].
- [43] D. Guo, A. Alexandru, R. Molina, M. Mai, and M. Döring, Extraction of isoscalar $\pi\pi$ phase-shifts from lattice QCD, Phys. Rev. D **98**, 014507 (2018), arXiv:1803.02897 [hep-lat].
- [44] T. Blum *et al.* (RBC and UKQCD Collaborations), Isospin 0 and 2 two-pion scattering at physical pion mass using all-to-all propagators with periodic boundary conditions in lattice QCD, Phys. Rev. D **107**, 094512 (2023), [Erratum: Phys. Rev. D **108**, 039902 (2023)], arXiv:2301.09286 [hep-lat].
- [45] A. Rodas, J. J. Dudek, and R. G. Edwards (Hadron Spectrum Collaboration), Quark mass dependence of $\pi\pi$ scattering in isospin 0, 1, and 2 from lattice QCD, Phys. Rev. D **108**, 034513 (2023), arXiv:2303.10701 [hep-lat].
- [46] M. Bruno, D. Hoying, T. Izubuchi, C. Lehner, A. S. Meyer, and M. Tomii, Isospin 0 and 2 two-pion scattering at physical pion mass using distillation with periodic boundary conditions in lattice QCD, arXiv:2304.03313 [hep-lat] (2023).
- [47] S. Navas *et al.* (Particle Data Group), Review of particle physics, Phys. Rev. D **110**, 030001 (2024).
- [48] D. Severt, M. Mai, and U.-G. Meißner, Particle-dimer approach for the Roper resonance in a finite volume, J. High Energy Phys. **2023** (04), 100, arXiv:2212.02171 [hep-lat].
- [49] R. G. Edwards and B. Joó (SciDAC, LHP and UKQCD Collaborations), The Chroma software system for Lattice QCD, Nucl. Phys. B Proc. Suppl. **140**, 832 (2005), arXiv:hep-lat/0409003 [hep-lat].
- [50] L. Barca, G. Bali, and S. Collins, Progress on nucleon transition matrix elements with a lattice QCD variational analysis, Proc. Sci. **EuroPLeX2023**, 002 (2024), arXiv:2405.20875 [hep-lat].

Supplemental Material

CONSTRUCTION OF THE TWO- AND THREE-POINT FUNCTIONS

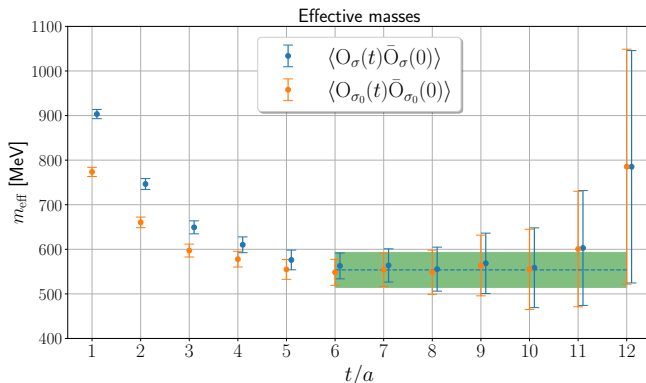


Figure S1: Effective masses of the two-point correlation functions constructed from the interpolators O_σ (orange points) and O_{σ_0} (blue points). The blue dashed line and green band indicate the mass, $m_\sigma = (554 \pm 39) \text{ MeV}$, extracted from a fit to $\langle O_{\sigma_0}(t)\bar{O}_{\sigma_0}(0) \rangle$ in the range $t/a = 6 - 12$.

We aim to improve the extraction of the scalar matrix element of the nucleon at rest by constructing improved three-point correlation functions (13) via the variational approach utilising bases including the standard proton interpolator (with a qqq structure) and S-wave proton-sigma interpolators (with a $qqq - \bar{q}q$ structure). For the latter, we combine a standard proton and a (scalar) sigma operator that are both projected onto zero momentum. For the two bases realised in the study (see Sec. III), we

implement the proton operator ($O_p(\mathbf{0})$) and three multi-particle interpolators

$$O_{p\sigma} = O_p(\mathbf{0})O_\sigma(\mathbf{0}), \quad (\text{S1})$$

$$O_{p\sigma_0} = O_p(\mathbf{0})O_{\sigma_0}(\mathbf{0}), \quad (\text{S2})$$

$$O_{p\sigma_8} = O_p(\mathbf{0})O_{\sigma_8}(\mathbf{0}). \quad (\text{S3})$$

The flavour content of the sigma operators corresponds to the SU(2) singlet (O_σ) and SU(3) singlet and octet ($O_{p\sigma_0}$ and $O_{p\sigma_8}$, respectively), combinations.

To improve the overlap with the lowest lying levels, the proton and sigma interpolators in the single and multi-particle operators are spatially extended. For the former, we apply the same quark field smearing as employed in [50], i.e., 150 Wuppertal smearing steps⁵ with $\alpha = 0.25$, corresponding to a smearing radius of $\langle r^2 \rangle^{1/2} \sim 1.0 \text{ fm}$ for the proton interpolator. Regarding the sigma meson interpolators, we investigated 5 different smearings: 0, 5, 20, 40 and 150 iterations. We find that 5 iterations, with a $\langle r^2 \rangle^{1/2} \sim 0.2 \text{ fm}$ for the interpolator, is sufficient to reduce excited state contributions to the two-point functions $C_{2\text{pt}}^{\sigma\sigma}(t) = \langle O_\sigma(t)\bar{O}_\sigma(0) \rangle$ and $C_{2\text{pt}}^{\sigma_0\sigma_0}(t) = \langle O_{\sigma_0}(t)\bar{O}_{\sigma_0}(0) \rangle$ such that the respective effective masses plateau around $t = 6a = 0.6 \text{ fm}$, see Fig. S1. Fitting to $C_{2\text{pt}}^{\sigma_0\sigma_0}(t)$ in the range $t/a = 6 - 12$ we obtain $m_\sigma = (554 \pm 39) \text{ MeV}$. A higher number of iterations increases the noise without further reducing the excited state contamination. Note that, as we are working in the SU(3) symmetric limit, there is no mixing between

⁵ The gauge links are APE smeared [35], see [15] for details.

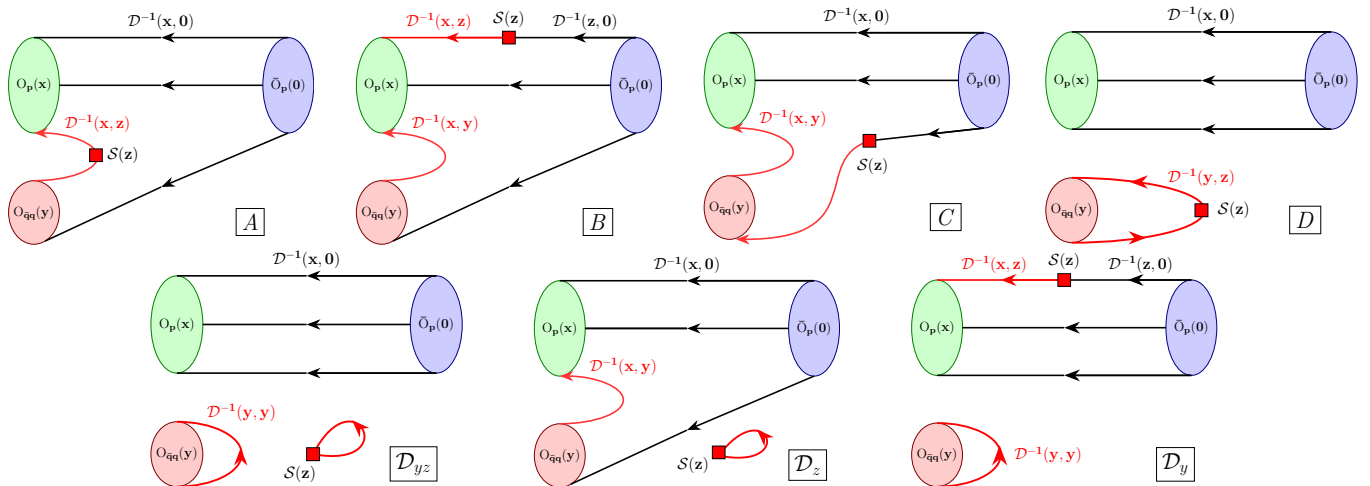


Figure S2: Topologies in position space arising from the Wick contractions of the three-point correlation functions $\langle O_{N\sigma}(x, y) \mathcal{J}(z) \bar{O}_p(0) \rangle$. The three black lines represent point-to-all propagators, the two red lines in each topology correspond to all-to-all propagators, and the red square indicates the current insertion at $z = (\mathbf{z}, \tau)$. The $O_{N\sigma}(x, y)$ interpolator contains a qqq -structure $O_p(x)$ at the spacetime position $x = (\mathbf{x}, t)$ and a $\bar{q}q$ -structure $O_{\bar{q}q}(y)$ at $y = (\mathbf{y}, t)$.

the singlet and octet flavour sectors. However, the spectrum of states created by the SU(2) singlet operator O_σ will include both singlet and octet levels. Concerning the σ_8 interpolator, we were not able to achieve a clear plateau in the respective two-point function for any of the 5 smearings realised.

In order to implement the variational approach, the two-point functions in Eq. (10) and the following three-point functions

$$\langle O_p(t) \mathcal{S}^q(\tau) \bar{O}_p(0) \rangle, \quad (\text{S4})$$

$$\langle O_{p\sigma}(t) \mathcal{S}^q(\tau) \bar{O}_p(0) \rangle, \quad (\text{S5})$$

$$\langle O_{p\sigma_0}(t) \mathcal{S}^q(\tau) \bar{O}_p(0) \rangle, \quad (\text{S6})$$

$$\langle O_{p\sigma_8}(t) \mathcal{S}^q(\tau) \bar{O}_p(0) \rangle, \quad (\text{S7})$$

need to be evaluated in the rest frame of the proton. We remind the reader that we neglect the $N\sigma \xrightarrow{S^q} N\sigma$ contributions to the GEVP-improved three-point functions (13). In the following, we restrict the discussion to the calculation of the correlation functions involving the proton-sigma interpolators. Furthermore, as the relevant two-point functions can be constructed from (S4)-(S7) replacing the scalar current with smeared scalar operators inserted at $\tau = 0$, we only consider the three-point functions (S5)-(S7). Figure S2 displays the quark-line diagram topologies which arise from the Wick contractions of these three-point functions. The connected diagrams A, B, and C and the connected parts involving the proton interpolator of the remaining diagrams are constructed from point-to-all and sequential propagators. Stochastic estimation is employed to compute the quark loops for diagrams \mathcal{D}_{yz} , \mathcal{D}_z , and \mathcal{D}_y and the one-end

trick is utilised to determine the local to smeared scalar two-point function in diagram D. To improve the determination of this diagram and also diagrams \mathcal{D}_{yz} and \mathcal{D}_y , we realise four source positions for the scalar two-point function and the proton two- and three-point functions. In total, we require the equivalent of ≈ 22 propagators for each source-sink separation. However, in order to investigate the efficacy of the variational approach and, in particular, to ensure a reliable extraction of the corresponding eigenvectors, we realise source-sink separations up to $t = 11a = 1.1$ fm. When taking the recycling of propagators into account, this means that we need ≈ 132 propagators overall per configuration for the GEVP analysis.

Finally, we remark that as the scalar operator has the quantum numbers of the vacuum, we implement the vacuum-subtracted current $\tilde{\mathcal{S}}^q = \mathcal{S}^q - \langle \mathcal{S}^q \rangle$ and interpolators $\tilde{O}_\sigma = O_\sigma - \langle O_\sigma \rangle$, $\tilde{O}_{\sigma_0} = O_{\sigma_0} - \langle O_{\sigma_0} \rangle$ and $\tilde{O}_{\sigma_8} = O_{\sigma_8} - \langle O_{\sigma_8} \rangle$. Also within the multi-particle interpolators, we replace $O_{p\sigma}$ with $\tilde{O}_{p\sigma} = O_p(O_\sigma - \langle O_\sigma \rangle)$ etc.

SUMMATION METHOD RESULTS

In this section, we present results for the summed ratios $R_{u+d,s}^{\text{sum}}$ (16) for both the GEVP-improved and standard correlation functions. Figure S3 displays the summed ratios obtained with $c = 2a$, where basis \mathbb{B}_2 is employed for the variational approach. Note that for this value of c , $R_{u+d,s}^{\text{sum}}$ is evaluated for $t \geq 4a$. The results for basis

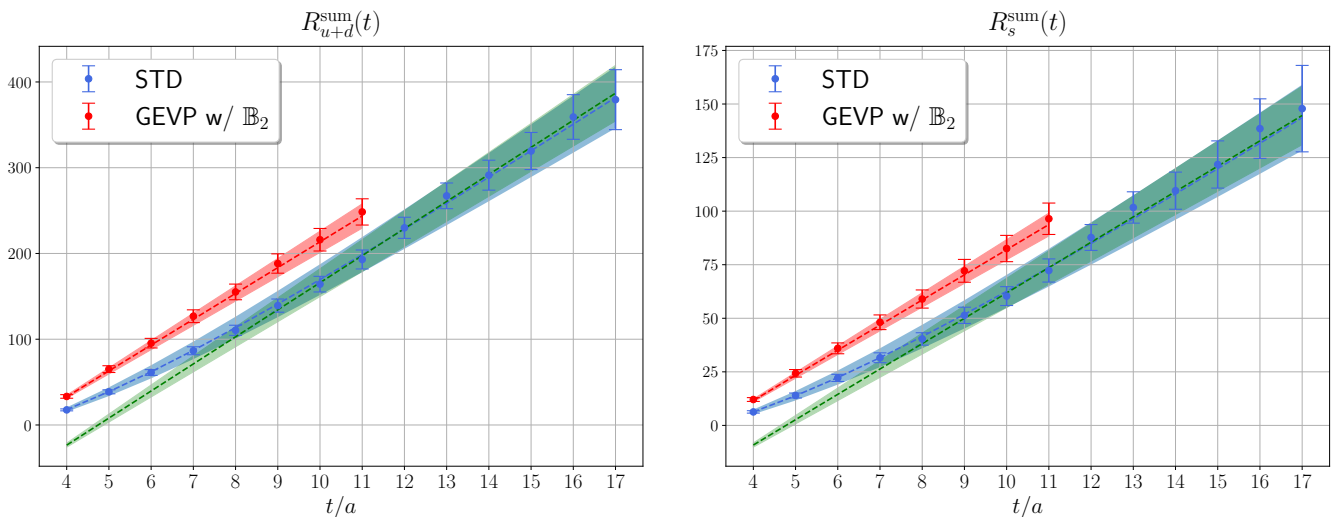


Figure S3: Results for the summed ratios, Eq. (16) with $c = 2a$, for the $u + d$ (left) and s (right) flavour combinations of the scalar current. The GEVP-improved results (red points) are obtained utilising basis \mathbb{B}_2 . The red dashed line and band indicate the central value and uncertainty of a linear fit (18) over the range $t/a = 4 - 11$. For the standard summed ratios (blue points) a linear fit for $t/a = 10 - 17$ (light green band) is displayed along with a fit including contributions from the first excited state (blue band) ((17) with $c_{11} = 0$) for $t/a = 4 - 17$.

\mathbb{B}_3 are consistent within errors. As seen in the figure, the standard $R_{u+d,s}^{\text{sum}}$ suffers from excited state contamination for $t < 8a = 0.8$ fm. In contrast, for the GEVP-improved $R_{u+d,s}^{\text{sum}}$, the $N\sigma$ contributions at short time separations are removed and ground state dominance sets in already at $t \approx 4a = 0.4$ fm. The fits performed reflect this behaviour. For the standard summed ratios, contributions from the ground state and a single excited state are mod-

elled using Eq. (17) when fitting in the range t_{\min} to t_{\max} with $t_{\min} = 4a - 6a$ and $t_{\max} = 17a$. For $t_{\min} \geq 8a$ a linear fit (18) is sufficient. Similarly, a linear fit to the GEVP-improved $R_{u+d,s}^{\text{sum}}$ for $t_{\min} \geq 4a$ with $t_{\max} = 11a$ gives a good fit quality. Representative examples of these fits are presented in Fig. S3. We remark that compatible values for the scalar charges are obtained when fitting to the summed ratios with $c = 3a$.